Spectroscopic Evidence for Interaction between Transmembrane Helices 3 and 5 in Rhodopsin†

Mareike Beck,‡,§ Thomas P. Sakmar,§ and Friedrich Siebert*,‡

Institut für Biophysik und Strahlenbiologie, Albert-Ludwigs-Universität, Albertstrasse 23, 79104 Freiburg, Federal Republic of Germany, and Laboratory of Molecular Biology and Biochemistry, The Howard Hughes Medical Institute, Rockefeller University, 1230 York Avenue, New York, New York 10021

Received January 21, 1998; Revised Manuscript Received March 23, 1998

ABSTRACT: Recent molecular models of rhodopsin (Rho) propose a specific interaction between transmembrane (TM) helices 3 and 5, which appears to be mediated by amino acid residues Glu^{122} and His^{211} on TM helices 3 and 5, respectively. To test this proposed interaction, four single-site histidine replacement mutants (H100N, H152N, H211N, and H211F), two single-site glutamic acid replacement mutants (E122Q and E122A), and three double-site replacement mutants (E122Q/H211F, E122Q/H211N, and E122A/H211F) of Rho were prepared. The expressed mutant pigments reconstituted into membranes were studied by FTIR difference spectroscopy addressing especially the transition to metarhodopsin I (MI). It is shown that the lipid environment influences bands typical of the MI state. Spectra of mutants with substituted Glu^{122} allowed assignments of the C═O stretch of protonated Glu^{122} in the dark state and in MI of Rho. Mutation of His^{211}, but not of other histidine residues, affects these vibrational modes assigned to Glu^{122}. In addition, replacements of His^{211} affect protein modes that are proposed to arise from a third, hydroxyl-bearing group, which also interacts with Glu^{122}. These modes are influenced as well when Glu^{122} is replaced by Ala in mutant E122A but not when it is replaced by Gln in mutant E122Q. These results provide direct experimental evidence for an interaction between TM helices 3 and 5 in Rho, which is mediated by Glu^{122} and His^{211}.

Rhodopsin (Rho)[1] is a member of the superfamily of seven-transmembrane-helical, G protein-coupled receptors (GPCRs) (*1*). The Rho chromophore, 11-*cis*-retinal, is covalently bound to the protein via a protonated Schiff base linkage (*2*) at Lys^{296} (*3*, *4*). After photoisomerization of the chromophore to *all-trans*-retinal, the protein relaxes through a series of spectrally defined intermediates to the active conformation (R*), which binds the heterotrimeric G protein transducin and thereby couples photon absorption to the biochemical cascade of visual transduction. R* is defined spectroscopically to be metarhodopsin II (MII) (*5*, *6*). MII (λ_{max} = 380 nm) exists in an equilibrium with its precursor metarhodopsin I (MI) (λ_{max} = 478 nm). The MI/MII equilibrium depends on temperature and pH. Acidic pH and higher temperature favor MII, whereas basic pH and lower temperature favor MI (*7*, *8*). The pK_a of the MI/MII transition is ≈6.5.

Site-directed mutagenesis of Rho in conjunction with infrared difference spectroscopy has shown that the Schiff base counterion, Glu^{113}, becomes protonated concurrently with deprotonation of the Schiff base (*9*, *10*). Chromophore isomerization and Schiff base deprotonation to form MII are further coupled to protein conformational changes at the cytoplasmic surface of the receptor that allow transducin to interact. It is of special interest to study the activation path of Rho from the chromophore isomerization as the primary event up to the deprotonation of the Schiff base, because it may provide some clues to the activation mechanism of other G protein-coupled receptors. In Rho, the chromophore *all-trans*-retinal can be regarded as a pharmacologic agonist, whereas 11-*cis*-retinal functions as a potent inverse agonist, completely shutting off the active state.

Electron cryomicroscopy has provided a map at moderate resolution of the three-dimensional arrangement of the seven membrane-spanning α-helices of Rho (*11*). The resolution of the electron density is still not sufficient to locate single amino acid residues or the chromophore. However, since the primary structures of the TM helices are known, concepts of molecular modeling have been applied using various constraints. In one model, possible common motifs for hydrogen bonding among a large number of G protein-coupled receptors are used together with some constraints on the position of the helices (*12*). In another model, the low-resolution model derived by Baldwin (*13*) is used together with the constraints on the interaction of the counterion Glu^{113} with the chromophore bound to Lys^{296} provided by solid-state NMR measurements of Rho and bathorhodopsin (*14*, *15*). In a refinement of that model, the

† This work was supported in part by DFG Grant Si 278/16-1 and SFB-60/G-13. T.P.S. is an Associate Investigator of the Howard Hughes Medical Institute. M.B. was supported by a fellowship of the state of Baden-Württemberg (LGFG).

* Author to whom correspondence should be addressed (telephone 49-761-203-5396; fax 49-761-203-5016; e-mail frisi@ruf.uni-freiburg.de).

‡ Albert-Ludwigs-Universität.

§ The Howard Hughes Medical Institute, Rockefeller University.

[1] Abbreviations: bp, base pairs; Con A, concanavalin A.; DM, *n*-dodecyl β-D-maltoside; FTIR, Fourier transform infrared; GPCR, G protein-coupled receptor; MI, metarhodopsin I; MII, metarhodopsin II; Rho, (wild-type) rhodopsin; TM, transmembrane.

S0006-2960(98)00156-1 CCC: $15.00
Published on Web 04/29/1998

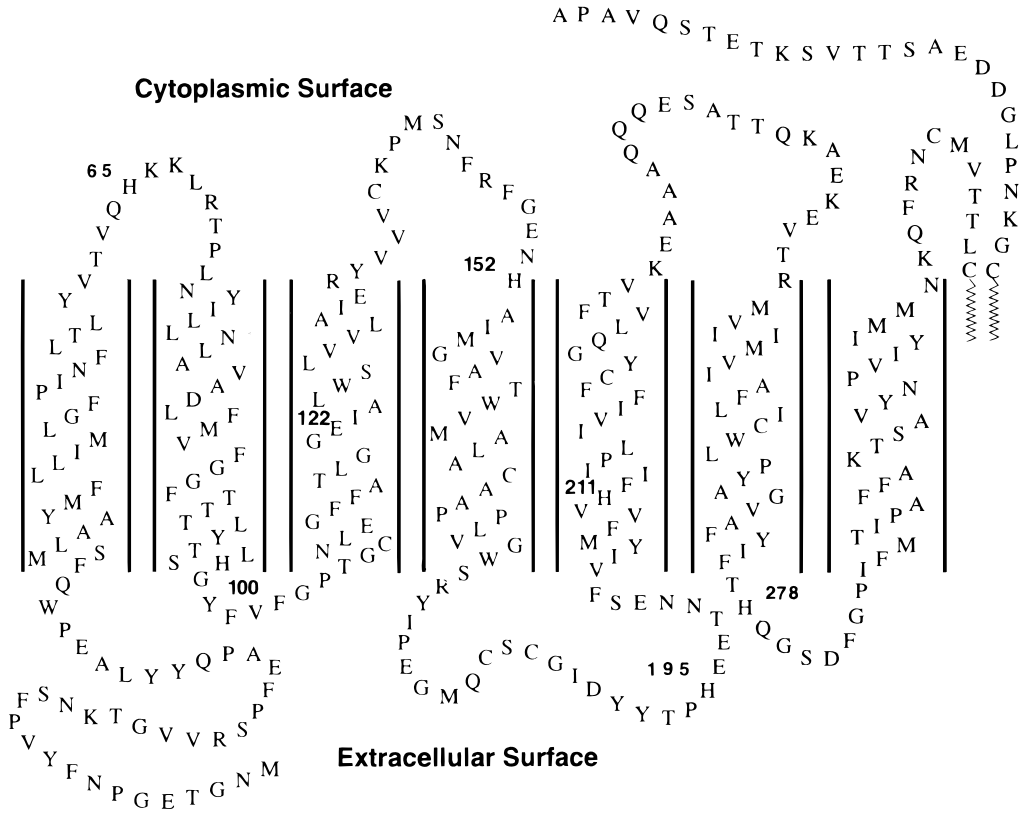

FIGURE 1: Secondary structural model of bovine Rho. The cytoplasmic surface and the extracellular surface of the receptor are above and below the seven TM helices, respectively. Each of the six histidine residues in the protein, and one of the glutamic acid residues (Glu^{122}), is numbered. His^{100}, His^{152}, His^{211}, and Glu^{122} were studied in this paper.

properties of several Rho mutants with replacements on TM helices 3 and 6 were considered (*16*). Although the two models (*12*, *16*) show considerable differences with respect to the orientation of the chromophore, they agree reasonably well with the three-dimensional electron density.

Rho activation involves protein conformation changes (*17*). A series of elegant studies using site-directed mutagenesis of Rho in combination with spin labeling and EPR spectroscopy showed that Rho activation after chromophore isomerization involves outward rigid body movements of TM helices 3 and 6 relative to the center of the helix bundle (*18*−*20*). Cross-linking of these helices near the cytoplasmic surface of the receptor by engineered disulfide bonds (*18*), or by chelated metal ions (*20*), prevents receptor activation. Movements of TM helices 3 and 6 are likely to cause changes in interhelical interactions among those helices in contact with 3 and 6. The derived electron projection density map demonstrates that TM helix 3 is significantly tilted relative to the other TM helices, providing the possibility for contact with TM helix 5 near the cytoplasmatic surface of the receptor. Both molecular models (*12*, *16*) predict the interaction between TM helices 3 and 5 and indicate that it may be mediated by Glu^{122} (TM helix 3) and His^{211} (TM helix 5). Fourier transform infrared difference (FTIR) spectroscopy, especially in combination with site-directed mutagenesis, has been shown to be a sensitive tool for detecting interactions among residues in Rho (*21*, *22*) and bacteriorhodopsin (*23*, *24*).

We measured FTIR difference spectra of nine Rho mutants with replacements of Glu^{122} and/or a His: four single-site histidine replacement mutants (H100N, H152N, H211N, and H211F), two single-site glutamic acid replacement mutants (E122Q and E122A), and three double-site replacement mutants (E122Q/H211F, E122Q/H211N, and E122A/H211F) (Figure 1). The mutant pigments were studied in membranes to facilitate the measurement of their MI difference spectra (MI, dark state) and to avoid the potential of distortion of spectral bands related to detergent. Glu^{122} bands can be definitively assigned in the MI difference spectrum of Rho. The data clearly demonstrate that His^{211} mutation, but not mutation of His^{100} or His^{152}, influences Glu^{122}. This influence may be transmitted via an additional group X, most likely bearing an OH function. The FTIR data provide strong experimental support for an interaction between Glu^{122} and His^{211} and support models of Rho structure in which TM helices 3 and 5 interact.

EXPERIMENTAL PROCEDURES

Materials. L-α-Lecithin from fresh egg yolk was from Fluka Chemie, and *n*-octyl β-D-glucoside was from Bachem Biochemica or Anatrace, Inc. Sources of other materials have been previously reported (*25*−*28*).

Preparation of Rho and Rho Mutants. Disk membranes were isolated from bovine rod outer segments, and Rho was solubilized and purified on a Con A−Sepharose column in *n*-octyl β-D-glucoside as described (*29*, *30*). Purified Rho was dialyzed against 1 mM sodium phosphate buffer (pH 6.5). Site-directed mutagenesis was accomplished using restriction fragment replacement in a synthetic gene for bovine Rho (*31*). Mutagenic synthetic DNA duplexes for single-site mutants were as follows: H100N, 68-bp *Bgl*II−*Rsr*II duplex; H152N, 86-bp *Spe*I−*BsaH*I duplex;

H211N and H211F, 75-bp *Pst*I−*Ava*II duplex; E122A, 63-bp *Spe*I−*Rsr*II duplex. The nucleotide sequences of all cloned synthetic duplexes were confirmed by the chain terminator method for DNA sequencing of purified plasmid DNA. Double-site mutants were assembled from the corresponding single-site mutants. The opsin genes were expressed in COS-1 cells and purified by immunoaffinity adsorption as previously described (*9*, *28*). To prepare recombinant pigments reconstituted into phospholipid vesicles by dialysis, the detergent *n*-octyl β-D-glucoside was used in place of *n*-dodecyl β-D-maltoside (DM). The octyl glucoside concentration was 2% (w/v) in the COS−cell solubilization buffer, and the purified pigments were obtained in 0.5 mM sodium phosphate (pH 6.5) and 1.5% (w/v) octyl glucoside.

Reconstitution of Rho and Mutant Pigments into Phospholipid Vesicles. Phosphatidylcholine (L-α-lecithin) from fresh egg yolk was lyophilized and resuspended in 1 mM sodium phosphate (pH 6.5). The suspension was incubated for 10 min in a bath sonicator and mixed with a purified Rho sample in a molar ratio of 100:1 (phospholipid/pigment). The samples were kept on ice for at least 1 h before dialysis. Samples were dialyzed against 1 mM sodium phosphate (pH 6.5) for 24 h at 8 °C with a 20 000 MW cutoff membrane in a microdialyzer unit (Pierce) in flow-through mode. Vesicles were pelleted by centrifugation at 80000*g* (4 °C, 16 h). Vesicles were washed and resuspended in a small volume of 1 mM sodium phosphate (pH 6.5). The concentration of pigment in the vesicles was determined by UV−visible spectroscopy.

FTIR Spectroscopy of Rho Mutants. Approximately 1.5 nmol of pigment in vesicles was adjusted to pH 8.5 by adding 0.5 μmol of sodium phosphate buffer and dried onto a CaF_2 window under a stream of N_2. Samples were rehydrated and sealed by another CaF_2 window. Measurements were performed with an IFS-28 interferometer (Bruker) equipped with a liquid N_2-cooled MCT detector. The degree of rehydration of the protein films was monitored by using the broad absorption band of water at ~3300 cm^{-1}. The degree of hydration was sufficient to yield full conversion to MII under the experimental conditions (i.e., 4 °C, pH 5.5). The spectral resolution was 2 cm^{-1}. Interferograms were averaged ($n = 512$) before and after illumination of the sample, and difference spectra were calculated from the single-channel spectra (*32*, *33*). Illumination was carried out by irradiation for 1 min with wavelengths above 530 nm (OG-530 filter, Schott) using a 150-W projector lamp. For mutant pigments with replacement of Glu^{122}, irradiation with wavelengths above 450 nm (OG-450 filter, Schott) was chosen. A home-built cryostat was used to cool the samples to −15 °C for measurement of MI difference spectra. The same procedure was used for measurement of the bathorhodopsin difference spectra, but the temperature of the sample was set at 80 K and illumination was carried out at wavelengths between 420 and 500 nm. In all figures showing direct difference spectra, the negative (dark state) band at 1390 cm^{-1}, which appears to be barely affected, if at all, by mutations, is used for approximate normalization.

FTIR Spectroscopy of 4(5)-Methylimidazole. Solutions of 10 mg/mL of 4(5)-methylimidazole were adjusted to pH 5.5 or 8.5 with HCl. Measurements were carried out at room temperature in a 5-mm-diameter cuvette with an optical path length of 4 μm. Water absorbance was subtracted such that the broad absorbance around 1650 cm^{-1} was eliminated.

Table 1: Spectral Properties of Mutant Pigments

mutant	λ_{max}[a] (nm)	blue shift[b] (cm^{-1})	mutant	λ_{max}[a] (nm)	blue shift[b] (cm^{-1})
H100N	499	40	E122Q	482	747
H152N	500	0	E122A	476	1008
H211N	495	202	E122Q/H211N	480	833
H211F	495	202	E122Q/H211F	480	833
			E122A/H211F	472	1186

[a] The λ_{max} value of Rho purified and measured under the same conditions was 500 nm. UV−visible spectroscopy was carried out as previously described (*21*). [b] Blue shift is defined as the difference in λ_{max} between the mutant pigment and Rho, in wavenumbers. The λ_{max} values of the mutant pigments agree well with previously published values (*25*, *34*, *35*, *37*).

RESULTS

UV−Visible Spectroscopy of Rho Mutants. Opsin and opsin mutants expressed in COS cells were regenerated with 11-*cis*-retinal, and the resulting pigments were purified in DM. Spectral properties of the mutant pigments are shown in Table 1. The λ_{max} values of mutants E122Q and E122A are significantly blue-shifted from that of Rho. These values agree well with those previously published for the same single-site mutants (*25*, *34*). The histidine replacement mutants H100N and H152N displayed λ_{max} values essentially identical to that of Rho, whereas mutants H211N and H211F displayed λ_{max} values that were only slightly blue-shifted. These results agree well with spectra taken under similar conditions as previously reported (*35*). The effect on the λ_{max} value of simultaneous mutation of Glu^{122} and His^{211} is nearly additive.

Transducin Activation by Mutant Pigments. The detailed biochemical properties of the mutants studied here will be presented elsewhere when the results of FTIR difference spectroscopy of the MII-like photoproducts of the mutants are reported. With the exception of the H211F mutant, all of the histidine mutants exhibited normal bleaching behavior and were capable of catalyzing GTPγS uptake by transducin as judged by a filter-binding assay (*36*). We observed altered bleaching and decreased activity of H211F (not shown). This effect may be due to abnormal bleaching in which the MI photoproduct is stablized relative to MII (*35*). However, a normal ability of mutant H211F to activate transducin was reported previously as well (*37*). Slight impairment of transducin activation by mutants E122A and E122Q was also reported previously (*25*, *34*). However, the salient result relevant to the present analysis is that each of the mutants is able to catalyze light-dependet GTPγS uptake by transducin, which indicates that the amino acid replacements do not introduce large perturbations in receptor structure.

FTIR Difference Spectrum of the MI Photoproduct of Rho. The infrared MI difference spectra of wild-type Rho in DM detergent and Rho reconstituted into phospholipid vesicles are compared in Figure 2. The spectrum of bovine Rho in rod outer segment disk membranes reported by Ganter et al. (*32*) is practically identical to the spectrum of wild-type Rho reconstituted into lipids (Figure 2). However, solubilization of Rho in DM detergent causes quite notable deviations in the spectrum above 1600 cm^{-1}. The positive bands at 1662 cm^{-1} (amide I) and near 1700 cm^{-1} (carbonyl of carboxylic acid group) (*32*) are greatly decreased. These spectral

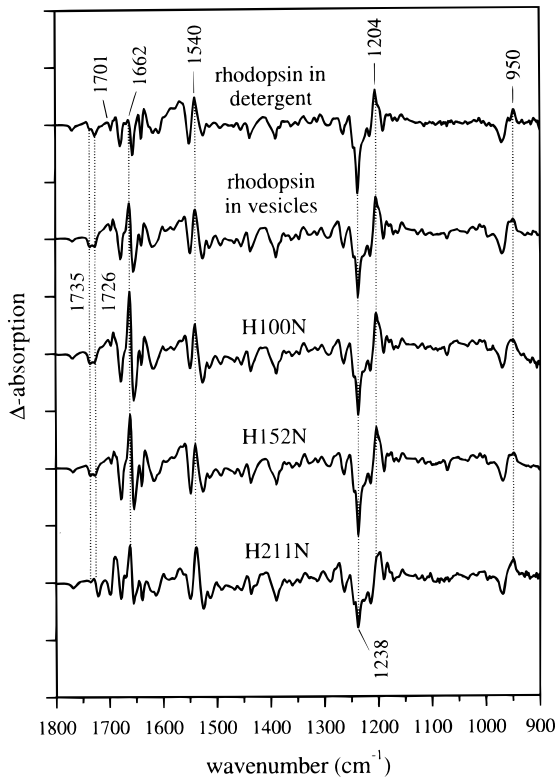

FIGURE 2: FTIR MI difference spectra (MI-dark state) of Rho solubilized in DM, Rho in lipid vesicles, and Rho mutants H100N, H152N, and H211N in lipid vesicles. The spectrum of Rho in detergent was obtained at −20 °C, pH 8.5. All spectra of pigments in lipid vesicles were obtained at −15 °C, pH 8.5. Absorption bands of the dark state are pointing downward; those of photoproduct point upward. Each tick interval on the ordinate scale corresponds to 0.0025 OD.

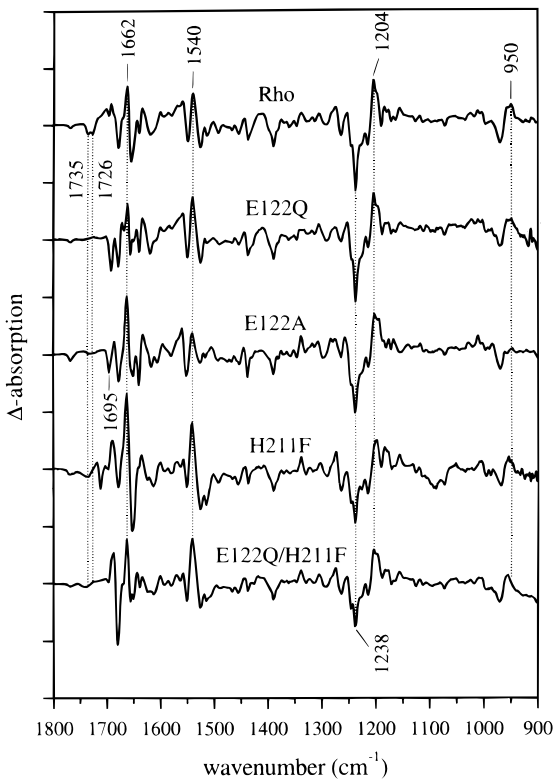

FIGURE 3: FTIR MI difference spectra (MI-dark state) of wild-type Rho and Rho mutants. Pigments were reconstituted into lipid vesicles. The spectra were obtained at −15 °C, pH 8.5. Spectra are normalized over the spectral region between 1500 and 900 cm^{-1} to compensate for different amounts of material. Each tick interval on the ordinate scale corresponds to 0.0025 OD.

differences may be explained in part by a lack of orientation of the detergent sample. However, the reconstituted lipid samples, which do not display these altered spectral features, are also not likely to be very well oriented. Therefore, we attribute the spectral differences mainly to altered protein conformations in MI due to differences in the protein environment in detergent versus membrane. Detergents are also known to affect the MI/MII equilibrium of photolyzed Rho. For example, MI is stabilized in digitonin and MII is stabilized in DM (*27*, *28*). These factors prompted us to perform FTIR measurements on samples reconstituted into lipid vesicles under conditions that allow MI-like photoproducts to be reproducibly stabilized. Every FTIR spectrum in this paper, other than that of Rho in detergent in Figure 2, is performed on a pigment sample in lipid vesicles.

FTIR Difference Spectra of Mutant Pigments H100N, H152N, H211N, and H211F. The spectra of the mutants H100N and H152N are essentially identical to the spectrum of Rho (Figure 2). Small variations in band intensities, but not band positions, are observed between 1680 and 1620 cm^{-1} (amide I bands). Since similar variations in band intensities were also frequently observed among different sample preparations of the same mutant, they do not reflect different structural features but are likely to be spectral artifacts due to the high background absorption. The spectrum of the mutant H211N shows several clear differences from that of Rho (Figure 2). They involve bands above 1660 cm^{-1} as well as features in the chromophore fingerprint region. In the fingerprint region, the 1238 cm^{-1} negative band in the H211N spectrum shows much lower intensity than the corresponding 1238 cm^{-1} band in the Rho spectrum. In addition, the positive band at 1204 cm^{-1} in the spectrum of H211N shows a small but significant downshift of its maximum compared to the corresponding band in the Rho spectrum. In this region, the spectrum of H211F (Figure 3) is very similar to that of H211N, with changes in the intensity of the 1238 cm^{-1} band and a downshift of the 1204 cm^{-1} band. The similarities between the H211N and H211F spectra suggest a common etiology for the spectral effects. These spectral features induced by mutation of His^{211} will be discussed in greater detail below. However, it is important to point out here that these changes in the fingerprint regions of the spectra of the His^{211} mutants are not noted in the spectra of H100N or H152N. The very good agreement between the spectra of Rho, H211N, and H211F in other regions demonstrates that no larger structural distortions are present in these mutant pigments.

FTIR Difference Spectra of Mutant Pigments E122Q, E122A, and E122Q/H211F. The MI difference spectra of the mutants E122Q, E122A, and E122Q/H211F together with the spectrum of Rho and appropriate controls are shown in Figure 3. Again, visual inspection of the spectra demonstrates that these mutants display no gross structural alterations due to the amino acid replacement(s). Spectral deviations can be seen above 1660 cm^{-1} for each of the mutants. Replacement of Glu^{122} (E122Q or E122A) causes qualitative differences in the amide I spectral range. Interestingly, in the E122Q/H211F spectrum, part of the change in the 1204 cm^{-1} band caused by replacement of His^{211} seems

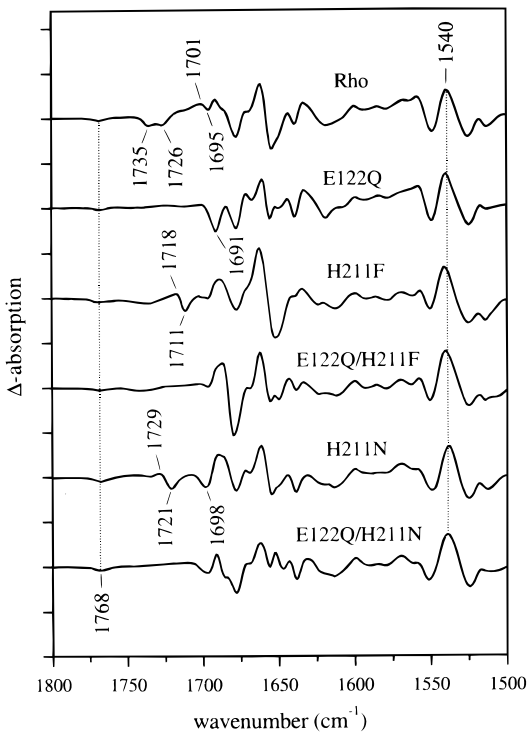

FIGURE 4: FTIR MI difference spectra (MI-dark state) in the spectral range between 1800 and 1500 cm^{-1}. The spectra for the range between 1800 and 900 cm^{-1}, except that of mutant E122Q/H211N, are shown in Figures 2 and 3. Each tick interval on the ordinate scale corresponds to 0.0025 OD.

to be reverted by the additional second-site replacement of Glu^{122}. The spectrum of E122A appears to be very similar to that of E122Q/H211F in this spectral range.

Influence of Glu^{122} Replacement on the Spectral Range above 1660 cm^{-1}. Figure 4 shows an enlarged view of relevant spectra in the 1800 to 1500 cm^{-1} range. Replacement of Glu^{122} by Gln abolishes all of the bands between 1740 and 1700 cm^{-1}, indicating that they are due to the C═O stretch of protonated Glu^{122}. The assignment of the double-band structure at 1735 and 1727 cm^{-1} to Glu^{122} was made previously on the basis of MII difference spectra measured in detergent (*9*). Thus, in the dark state of Rho, Glu^{122} is characterized by two C═O stretching bands at 1735 and 1726 cm^{-1}, which in MI merge together into the single band with a maximum at 1701 cm^{-1} (Figure 4). This low band position (1701 cm^{-1}) shows that Glu^{122} is strongly hydrogen bonded in MI. The assignment of the 1701 cm^{-1} band to a carboxyl group has been made earlier on the basis of the deuteriation-induced downshift (*32*), but the assignment of the band to a specific group (Glu^{122}) can now be made with the use of site-directed mutants. The double-band structure (1735/1726 cm^{-1}) indicates the possibility of heterogeneity. It is interesting to note that only the band at 1735 cm^{-1} undergoes the deuteriation-induced downshift. The downshifted 1735 cm^{-1} band is thereby superimposed onto the band at 1726 cm^{-1}, which does not exhibit a deuteriation-induced downshift (*32*).

The negative band at 1691 cm^{-1} in the spectrum of E122Q probably reflects the C═O stretch of Gln^{122} in the mutant pigment. The band superimposes onto a band located at 1695 cm^{-1} that can be seen in the spectrum of E122A (Figure 3) and is also present in the spectrum of Rho with low intensity due to its superposition with the band at 1701 cm^{-1}. Due to the overlap with amide I modes, it is not easy to determine to where the C═O group of Gln^{122} shifts in MI. In any case, from the spectra in Figure 4 we can exclude an upshift. It could be that the C═O group of Gln^{122} in the E122Q mutant causes the increase of the shoulder around 1675 cm^{-1}, which would indicate a considerable downshift similar to that observed for the C═O band of Glu^{122} in Rho.

Influence of His^{211} Replacement on the Spectral Range above 1660 cm^{-1}. The spectra of H211N (Figure 2) and H211F (Figure 3) clearly display changes in the range above 1660 cm^{-1}. Figure 4 shows an enlarged view of relevant spectra in the 1800 to 1500 cm^{-1} range. Mutation of His^{211} clearly causes alterations in the spectral region of protonated carboxyl groups. In the spectrum of H211F, a differential band appears at 1711(−)/1718(+) cm^{-1}. In the spectrum of H211N, a similar band structure is observed at 1721(−)/1729(+) cm^{-1}. These spectral features disappear upon second-site replacement of Glu^{122} with Gln in both double-site mutants E122Q/H211F and E122Q/H211N (Figure 4). This shows that the new differential bands apparent in the spectra of both single-site His^{211} mutants are caused by Glu^{122}. Thus, the environment of the Glu^{122} carboxyl group is drastically altered by mutation of His^{211} both in the dark state and in MI. In the spectra of the single-site His^{211} mutants, the double-band structures are replaced by a single band that is downshifted to 1711 and 1721 cm^{-1} in H211F and H211N, respectively. Instead of the strong hydrogen bonding of Glu^{122} observed in MI for wild-type Rho, upshifts to 1718 and 1729 cm^{-1} are observed in the spectra of H211F and H211N, respectively.

Both His^{211} replacements cause qualitatively similar spectral changes that depend in detail and magnitude on the newly introduced amino acid as might be expected. For example, the negative 1698 cm^{-1} band in the H211N mutant might be caused by the C═O stretching vibration of Asn^{211}. However, a definite assignment cannot be made for this mode in the H211N photoproduct due to overlap with amide I modes.

Bathorhodopsin Difference Spectrum (Batho-Dark State) of Mutant H211N. It was noted above that the positive band at 1204 cm^{-1} in the MI spectrum of Rho shows a small but significant downshift of its maximum in both mutants H211N and H211F (Figures 2 and 3). The intensities of the 1238 cm^{-1} bands are also reduced in these mutants. The question arises as to whether any changes in this chromophore fingerprint region of the spectrum are due to His^{211} mutation directly or to effects on chromophore bands that are influenced indirectly by the mutation. To address this question, we recorded the FTIR difference spectrum of the low-temperature photoproduct of mutant pigment H211N. We chose to compare this spectrum to that of bathorhodopsin since protein alterations are expected to contribute very little to the corresponding conformational transitions represented by the spectra. Therefore, an influence of His^{211} mutation on the chromophore would be easiest to detect. The low-temperature difference spectrum of the H211N mutant is compared with that of Rho in Figure 5. Under these conditions at a temperature of 80 K, the mutant photoproduct corresponds to bathorhodopsin as confirmed by a comparison of the spectra. The strong bands between 1150 and 1300 cm^{-1} are chromophore bands. The two prominent bands at 1238 cm^{-1} (−) and 1207 cm^{-1} (+) in the Rho difference

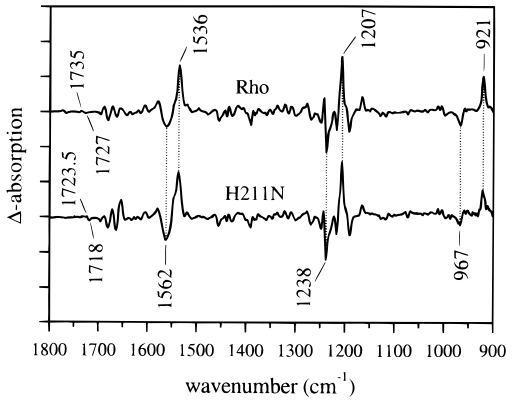

FIGURE 5: FTIR bathorhodopsin difference spectra (Batho, dark state) of wild-type Rho and Rho mutant H211N. Spectra were obtained at −180 °C, pH 5.5. Each tick interval on the ordinate scale corresponds to 0.0025 OD.

spectrum are noted at the same positions and with the same relative intensities in the spectrum of the H211N mutant. Thus, the intensities of the 1238 cm^{-1} band of the dark state and the 1207 cm^{-1} band of the bathorhodopsin state are not altered by mutagenesis of His^{211}. These results suggest that replacement of His^{211} does not affect the bands arising from the chromophore in the 1150 to 1300 cm^{-1} region of the spectrum. We can infer that spectral changes in this region in subsequent photoproducts are due to effects of mutation of His^{211} on protein conformation as discussed below.

Double-Difference FTIR Spectra. To elucidate subtle spectral changes caused by mutation, we subtracted individual spectra of mutant pigments from the spectrum of Rho. The vast majority of bands, which are not influenced by mutation, should cancel to give a flat baseline. Only bands arising either directly or indirectly from a particular amino acid replacement will appear in the double-difference spectrum after subtraction. The choice of the subtraction constant is critical since the spectra of two different samples with different absorbances must be subtracted. We evaluated the spectral range between 1125 and 1000 cm^{-1} and between 1250 and 1500 cm^{-1}, and especially the band at 1390 cm^{-1}, to minimize residual bands by subtraction. The subtraction constant varied between 0.92 and 1.12, in agreement with the approximately equal amounts of recombinant pigment in each infrared sample. Furthermore, difference spectra are subtracted in which the absorbance due to bulk water does not appear. The relative amounts of protein and water in the samples play a role only as far as the generation of MI is concerned, which is guaranteed as described under Experimental Procedures. The results of the subtractions (Rho − mutant) in the spectral range of 1000 to 1400 cm^{-1} for each of the mutants are shown in Figure 6. The uppermost trace in Figure 6 represents the subtraction for the H100N mutant (Rho − H100N). The reasonably flat line shows that the subtraction procedure is acceptable and confirms that the H100N replacement does not affect the FTIR spectrum of the H100N mutant, as suggested by comparison of the H100N and Rho spectra shown in Figure 2. In the subtraction for mutant H211F (Rho − H211F), two bands clearly show up at 1205 cm^{-1} (positive) and at 1236.5 cm^{-1} (negative). These bands are reproduced in the subtraction for mutant H211N. The observation that the spectral effects are independent of the particular amino acid

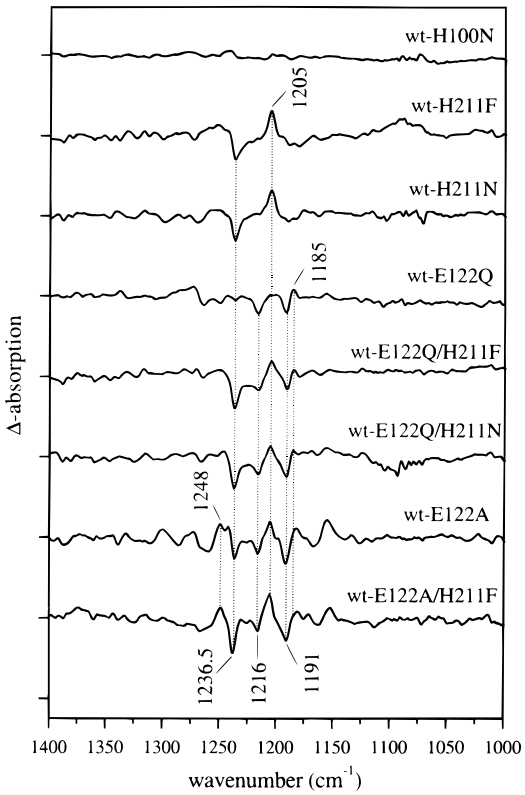

FIGURE 6: Subtractions of MI difference spectra in the region between 1400 and 1000 cm^{-1}. Mutant spectra were subtracted from the wild-type spectrum such that the differences were minimized over the spectral range from 1500 to 1250 cm^{-1} and from 1125 to 1000 cm^{-1}. Each tick interval on the ordinate scale corresponds to 0.0025 OD.

introduced in place of His^{211} suggests that the bands observed in the subtraction are due to His^{211}, although an indirect influence involving another group would still be consistent with the finding.

Since His^{211} mutation influences bands assigned to Glu^{122} as described above, a reciprocal effect of Glu^{122} mutation upon bands potentially attributable to His^{211} might also be expected. Therefore, we performed spectral subtractions for single-site mutants E122Q and E122A and for double-site mutants E122Q/H211F, E122Q/H211N, and E122A/H211F (Figure 6). It is clear that bands different from those observed for His^{211} mutation appear in the double-difference spectra. These include two negative bands at 1216 and 1191 cm^{-1} and a small positive one at about 1185 cm^{-1}. (The band structure around 1275 cm^{-1} observed for mutant E122Q probably represents an artifact, since it is not observed for the corresponding double mutants.) Furthermore, the subtracted spectra for the double-site mutants demonstrate that the effects of the single replacements are independent and additive. Thus, the mutation of His^{211} influences Glu^{122}, but Glu^{122} mutation does not influence bands that become apparent after His^{211} mutation. Whether or not these bands can be assignable to His^{211} will be discussed below.

DISCUSSION

Several molecular models of the transmembrane structure of Rho have been reported (*12*, *16*, *38*). Although prepared using different methodologies, these models are based upon electron density projection maps obtained from Rho recon-

stituted into phospholipid bilayers (*39*). The density maps were reconciled with existing primary structures and biochemical and mutagenesis experiments from a large number of related G protein-coupled receptors to give a convincing assignment of the seven helical segments to projection densities (*13*, *40*). In the case of Rho, 11-*cis*-retinal was oriented into the ligand-binding pocket of the receptor on the basis of NMR constraints that position the Glu^{113} counterion relative to the chromophore (*15*). This model of the helical bundle of Rho, which includes the 11-*cis*-retinal chromophore, is consistent with several spectroscopic and biochemical studies (*41*−*44*).

One particularly interesting observation present in molecular models of Rho is a predicted interaction between TM helices 3 and 5. At the extracellular surface of the receptor, the seven helices are arranged in a sequential orientation around a central open pocket. A significant tilt of TM helix 3 with respect to the helical bundle results in a change in the arrangement of the helices in moving from extracellular to cytoplasmic sides of the membrane domain. At the cytoplasmic surface of the receptor, TM helix 3 is much more central in location. Although not juxtaposed near the extracellular surface of the receptor, TM helix 3 appears close to TM helices 5 and 6 at the cytoplasmic surface. A specific interaction mediated by the chromophore between Gly^{121} on TM helix 3 and Phe^{261} on TM helix 6 has been demonstrated (*43*). In terms of interactions between TM helices 3 and 5, molecular models indicate a potential interaction between Glu^{122} (TM helix 3) and His^{211} (TM helix 5). It has also been pointed out that these residues are pairwise conserved in Rho pigments (*12*), meaning that the presence of a glutamic acid residue on TM helix 3 is accompanied by a histidine residue on TM helix 5.

The combination of site-directed mutagenesis and FTIR spectroscopy has provided valuable site-specific structural information about Rho and Rho mutants (*9*, *45*). In particular, spectral band assigments for the C═O stretching vibrations of carboxylic acid residues, including Glu^{122} (*9*) and Asp^{83} (*9*, *45*), have been propopsed. We undertook a study to evaluate the detailed role of histidine residues in Rho structure and function by the same general methodology. In addition, we combined histidine and glutamic acid mutations to test directly whether Glu^{122} and His^{211} interact in the dark state of Rho and its photoproducts. These studies are relevant for understanding the role of interhelical interaction between TM helices 3 and 5 in the function of Rho.

We prepared four single-site histidine replacement mutants (H100N, H152N, H211N, and H211F), two single-site glutamic acid replacement mutants (E122Q and E122A), and three double-site replacement mutants (E122Q/H211F, E122Q/H211N, and E122A/H211F). These mutant pigments were expressed at high levels, purified, and reconstituted in lipid membranes to measure FTIR difference spectra of their MI-like photoproducts. The study of the MI state was chosen in part to elucidate the postulated role of histidine residues in the MI/MII equilibrium. The FTIR difference spectrum of MI in reconstituted vesicle membranes was identical to that obtained from ROS disk membranes. The differences between the spectra of Rho obtained in detergent and membranes are presented above (Figure 2). All spectra of mutant pigments were recorded on samples reconstituted into membranes. This method proved particularly useful for the study of the MI photoproduct, which is difficult to trap in pigment samples in the presence of most detergents.

The FTIR difference spectra of the MI-like photoproducts of H100N and H152N were nearly identical to the spectrum of wild-type MI (Figure 2). This result clearly shows that replacement of either His^{100} at the extracellular border of TM helix 2, or His^{152} at the cytoplasmic border of TM helix 4, does not affect the structural determinants of MI as represented by even the fine detail of the FTIR difference spectra. These spectra will not be discussed further. The remainder of the discussion will focus on the interpretation of the FTIR spectra of the His^{211} mutants. There are two main effects of replacement of His^{211} represented in the FTIR spectra. First, His^{211} mutation affects the spectral region above 1660 cm^{-1}, a region associated with the C═O stretching frequencies of carboxyl groups. Second, His^{211} mutation affects the 1250 to 1150 cm^{-1} spectral range, a region generally associated with the chromophore fingerprint.

As presented above, inspection of the spectra of the E122Q mutant shows that the 1735/1726 cm^{-1} double band in the Rho spectrum (Figures 3 and 4) can be assigned to Glu^{122}. In MI, the two bands merge together into a single band at 1701 cm^{-1}, which indicates that Glu^{122} is strongly hydrogen-bonded in MI. The behavior of the 1735 cm^{-1} band in ^2H_2O has been previously reported (*32*, *46*). The 1735 cm^{-1} band, but not the 1726 cm^{-1} band, is sensitive to deuteriation. A tentative molecular interpretation of these band patterns is possible. The sensitivity of the C═O stretching frequency of the carboxyl group of Glu^{122} to deuteriation is caused by coupling of the OH-bending vibration to this mode, shifting it up by several wavenumbers. Deuteriation abolishes the coupling since the O^2H-bending vibration has a much lower frequency. Therefore, the C═O stretch shifts down to its uncoupled position. This indicates that the low-frequency part of the C═O stretch of Glu^{122} in dark Rho behaves as an uncoupled mode, although the carboxyl group is protonated. Since the extent of coupling between two vibrations depends not only on the frequency separation but also on geometric factors, the uncoupled character of the low-frequency part can be explained by an orientation of the hydrogen out of the OCO plane, largely eliminating the interaction of the two modes. Only isotopic labeling of glutamic acids in Rho could unequivocally rule out the possibility that the band at 1727 cm^{-1} is due to another group. However, since the splitting is abolished for all mutations that affect the band due to Glu^{122} [i.e., E122D (not shown), E122Q, E122A, H211F, and H211N], we regard this possibility as highly unlikely.

Interestingly, mutation of His^{211} also causes spectral alterations in the region above 1660 cm^{-1} (Figure 4). Differential bands are seen at 1711(−)/1718(+) and 1721(−)/1729(+) cm^{-1} in mutants H211F and H211N, respectively. The bands are abolished by the second-site replacement E122Q in the mutants E122Q/H211F and E122Q/H211N, indicating that the bands are caused by Glu^{122}. From a comparison of the positions of these bands to those corresponding to Glu^{122} in the wild-type Rho spectrum, it is clear that replacement of His^{211} significantly alters the environment of Glu^{122} in both the dark state and the photoproduct. These results provide direct experimental evidence of interaction between Glu^{122} and His^{211}. It is not

clear from this analysis alone whether His^{211} interacts directly with Glu^{122} or whether the influence is indirect and involves another side chain.

The other spectral changes evoked by His^{211} mutation are apparent as relatively subtle changes between 1250 and 1150 cm^{-1} (Figures 2 and 3). In the difference spectrum of Rho, the largest bands in this region at 1238 and 1204 cm^{-1} are caused by the chromophore (*32*). In the spectra of H211N and H211F, the magnitude of the 1238 cm^{-1} band is decreased and the maximum of the 1204 cm^{-1} band is downshifted slightly. To elucidate the subtle changes in this spectral region caused by mutation, mutant spectra were subtracted from Rho spectra as described above to produce the traces shown in Figure 6. The validity of this approach is demonstrated by the subtraction of the H100N spectrum from that of Rho, which gives essentially a flat line in the 1400 to 1000 cm^{-1} range (Figure 6), indicating that the mutation does not affect this region of the spectrum.

Two main bands are detected after subtraction of the spectra of the His^{211} mutants from the spectrum of Rho. These bands, at 1205 and 1236.5 cm^{-1}, appear at almost the same positions as chromophore bands in the MI difference spectra. Therefore, one could argue that the bands attributed to His^{211} are actually chromophore bands that are influenced by the mutation. To address this question, we compare the bathorhodopsin difference spectrum of the H211N mutant with that of Rho in Figure 5. The relative intensity of the strong chromophore bands between 1150 and 1300 cm^{-1} is not changed by the mutation, and the intensities of the 1238 cm^{-1} band of the dark state and of the 1207 cm^{-1} band of bathorhodopsin are not altered. Because the largest chromophore alterations occur in the transition to bathorhodopsin, we can exclude that the band at 1236.5 cm^{-1} obtained in the subtractions shown in Figure 6 represents a chromophore band. Therefore, it is also very unlikely that the positive band at 1205 cm^{-1} can be attributed to the chromophore. Otherwise, we would expect to observe an influence of the mutation on the bathorhodopsin band at 1207 cm^{-1}.

Having excluded chromophore contributions, we can assign the two bands at 1236.5 and 1205 cm^{-1} to groups of the protein. Taking into account that both His^{211} mutations produce the same band pattern in the subtraction, it would be reasonable to assign these bands to His^{211}, which might undergo a change in interaction in the transition to MI. We therefore recorded infrared spectra of 4(5)-methylimidazole as a model compound for the side chain of histidine (not shown). Characteristic bands were observed between 1200 and 1300 cm^{-1}, which had the highest intensity among the modes. However, we observed that these bands are very insensitive to the environment. This finding agrees with quantum chemical calculations showing that these modes are ring-stretching vibrations coupled to CH-bending vibrations (*47*). Only the NH-bending vibration located between 1100 and 1200 cm^{-1} is strongly influenced by the environment. However, this band was quite broad and displayed a very low infrared intensity. In contrast, the band is much stronger in Raman measurements (*47*). A rough estimate based on the measured molar absorbance clearly indicates that the intensities of the bands at 1205 and 1236.5 cm^{-1} in the H211F and H211N subtracted difference spectra (Figure 6) are far higher than would be calculated for a single imidazole side chain. According to the quantum chemical calculations (*47*), only the tautomerization (i.e., the change of the position of the NH group) could induce such large shifts on the ring vibrations. However, in such a case, three bands undergoing shifts must show up in the subtraction. Therefore, we regard it as unlikely, although we cannot completely exclude it, that the bands in Figure 6 that appear upon His^{211} mutation are actually histidine bands.

Thus, we assign the 1205 and 1236.5 cm^{-1} bands to another group. The band position would be in agreement with the C−O stretching vibration of an OH-bearing residue (group X) undergoing a change in hydrogen bonding. Group X must be held by His^{211} in a position making it sensitive to the MI transition. If His^{211} is replaced, group X no longer participates in the transition. Since His^{211} mutation also affects the C═O stretch of Glu^{122}, inducing an upshift in MI instead of the strong downshift observed for wild-type Rho, and also since the band assigned to group X undergoes a large shift, it appears reasonable to assume that the interaction of group X with Glu^{122} is abolished by the His^{211} mutation, thereby causing the changes in the C═O stretching mode of Glu^{122}. We have assigned the bands of group X to the dark state and MI of wild-type Rho. This appears plausible since the bands show up irrespective of whether His^{211} is replaced by an Asn or a Phe. If the bands do in fact represent a histidine vibration, they would, of course, characterize the two states of wild-type Rho.

The E122Q mutation causes two negative bands and one positive band in the subtracted spectrum (Figure 6). We tentatively assign these bands to the C−O stretching vibration of Glu^{122}. (The positive band at 1185 cm^{-1} has very low intensity, making it difficult to identify with certainty. Thus, it could be that the photoproduct band cannot be detected.) The two negative bands could correspond to the two negative bands observed for the corresponding C═O stretching vibration.

The preceding discussion logically presents the following situation. His^{211} mutation influences the C═O stretching band of Glu^{122} and a mode (probably C−O stretch) of an unidentified group X. The influence on the C═O stretch is thought to be mediated via group X (e.g., hydrogen bonding of the OH group of group X to the carbonyl). However, group X does not, according to the tentative assignment, influence the C−O stretching mode of Glu^{122}. In addition, E122Q mutation does not influence the bands of group X. To resolve this apparent contradiction, one has to keep in mind that Gln^{122} in mutant E122Q bears a C═O group, as does Glu^{122} in Rho. Thus, it could be that group X interacts with the C═O group of Glu^{122} or Gln^{122} in the same way. Therefore, the bands attributed to group X are not altered by the E122Q mutation. If His^{211} is removed, this interaction is no longer present, and the C═O group of Glu^{122} experiences a completely altered environment in both the dark state and in MI. This interaction would not necessarily influence the C−O stretching mode. The C═O band of Gln^{122} of the dark state has been assigned to the negative band at 1691 cm^{-1}, and we have provided evidence that it is not upshifted in MI. The band may be considerably downshifted, causing the pronounced shoulder at 1675 cm^{-1} (Figure 4). Thus, it seems that with respect to the C═O group, the behavior of Gln^{122} in E122Q is not very different from that of Glu^{122} in Rho.

One way to test the proposed interaction with the C═O group is to eliminate it by replacing Glu^{122} by Ala. The yield of the reconstituted E122A mutant was consistently lower than that of other pigments so that the signal/noise ratio is reduced in its FTIR spectra. In the description of Figure 3, we have already noted that between 1150 and 1250 cm^{-1} the spectrum of the E122A mutant is very similar to that of the double mutants E122Q/H211F(N). The subtracted spectra are shown in Figure 6. For the double-site mutant E122A/H211F, the band pattern observed with mutant E122Q/H211F is reproduced. In addition, a positive band shows up at 1248 cm^{-1}. However, most notably, even within the reduced signal/noise ratio, the same pattern is readily seen as with the subtraction for the single mutant E122A. Thus, the bands attributed to group X are influenced by the E122A mutation. Together with the previous discussion, this indicates that group X interacts with the C═O group of Glu^{122} (or Gln^{122} in E122Q). The additional positive band observed at 1248 cm^{-1} (Figure 6) may be caused by group X in the E122A mutant. It is interesting to note that most of the bands between 1150 and 1250 cm^{-1} attributed to group X and Glu^{122} do not show up in the MII spectra (Beck, Sakmar, and Siebert, unpublished observation). This finding agrees with the observation that the strong downshift of the C═O band of Glu^{122} is reverted in MII and instead a small upshift takes place.

In summary, our data clearly demonstrate that His^{211} mutation influences Glu^{122}. We have provided evidence that this influence is transmitted via an additional group X, most likely bearing an OH function. However, we still cannot completely exclude that His^{211} interacts directly with Glu^{122}. At present, the assignment of bands to group X is only tentative. We cannot completely exclude that the corresponding bands are due to His^{211}. Even if the bands are due to group X, interaction between His^{211} and Glu^{122} would still be possible. The strongest infrared bands of a histidine are not sensitive to such an interaction. Therefore, the histidine would not show up in the FTIR difference spectrum, although its interaction is changed in the transition to MI. In any case, since the spectral effects can be explained only if His^{211} is close to Glu^{122}, we can conclude that TM helices 3 and 5 come close together near the level of these two positions in the bilayer. These data support the α-carbon model of G protein-coupled receptors based on structural data from Rho, which shows that α-carbons corresponding to Glu^{122} and His^{211} are separated by only ∼10.9 Å (*40*). In addition, the FTIR data provide strong experimental support for the spatial arrangement of the amino acid chains deduced by the two different procedures of molecular modeling that have proposed an interaction between Glu^{122} and His^{211} (*12*, *16*). Thus, this FTIR investigation on recombinant rhodopsins has provided additional important structural constraints. Ongoing investigations with additional mutants may clarify the identity of group X and further determine the structural basis of the activation pathway of Rho and related G protein-coupled receptors. The specific role of histidines for the formation of MII will be treated in a separate paper.

ACKNOWLEDGMENT

We thank S. W. Lin, K. Fahmy, T. Chan, T. Zvyaga, J. Isele, and S. O. Smith for helpful discussions.

REFERENCES

1. Sakmar, T. P. (1998) *Prog. Nucleic Acid Res. Mol. Biol. 59*, 1−34.
2. Oseroff, A. R., and Callender, R. H. (1974) *Biochemistry 13*, 4243−4248.
3. Hargrave, P. A., McDowell, J. H., Curtis, D. R., Wang, J. K., Juszczak, E., Fong, S.-L., Mohanna-Rao, J. K., and Argos, P. (1983) *Biophys. Struct. Mech. 9*, 235−244.
4. Ovchinnikov, Y. A. (1982) *FEBS Lett. 148*, 179−191.
5. Emeis, D., Kühn, H., Reichert, J., and Hofmann, K. P. (1982) *FEBS Lett. 143*, 29−34.
6. Kibelbek, J., Mitchell, D. C., Beach, J. M., and Litman, B. J. (1991) *Biochemistry 30*, 6761−6768.
7. Matthews, R. G., Hubbard, R., Brown, P. K., and Wald, G. (1963) *J. Gen. Phys. 47*, 215−240.
8. Radding, C. R., and Wald, G. (1956) *J. Gen. Phys. 39*, 909−923.
9. Fahmy, K., Jäger, F., Beck, M., Zvyaga, T. A., Sakmar, T. P., and Siebert, F. (1993) *Proc. Natl. Acad. Sci. U.S.A. 90*, 10206−10210.
10. Jäger, F., Fahmy, K., Sakmar, T. P., and Siebert, F. (1994) *Biochemistry 33*, 10878−10882.
11. Unger, V. M., Hargrave, P. A., Baldwin, J. M., and Schertler, G. F. X. (1997) *Nature 389*, 203−206.
12. Pogozheva, I. D., Lomize, A. L., and Mosberg, H. I. (1997) *Biophys. J. 70*, 1963−1985.
13. Baldwin, J. M. (1993) *EMBO J. 12*, 1693−1703.
14. Han, M., DeDecker, B. S., and Smith, S. O. (1993) *Biophys. J. 65*, 899−906.
15. Han, M., and Smith, S. O. (1995) *Biochemistry 34*, 1425−1432.
16. Shieh, T., Han, M., Sakmar, T. P., and Smith, S. O. (1997) *J. Mol. Biol. 269*, 373−384.
17. Ganter, U. M., Charitopoulos, T., Virmaux, N., and Siebert, F. (1992) *Photochem. Photobiol. 56*, 57−62.
18. Farrens, D. L., Altenbach, C., Yang, K., Hubbell, W. L., and Khorana, H. G. (1996) *Science 274*, 768−770.
19. Farahbakhsh, Z. T., Ridge, K. D., Khorana, H. G., and Hubbell, W. L. (1995) *Biochemistry 34*, 8812−8819.
20. Sheikh, S., Zvyaga, T. A., Lichtarge, O., Sakmar, T. P., and Bourne, H. R. (1996) *Nature 383*, 347−350.
21. Zvyaga, T. A., Fahmy, K., Siebert, F., and Sakmar, T. P. (1996) *Biochemistry 35*, 7536−7545.
22. Fahmy, K., Zvyaga, T. A., Sakmar, T. P., and Siebert, F. (1996) *Biochemistry 35*, 15065−15073.
23. Weidlich, O., Schalt, B., Friedman, N., Sheves, M., Lanyi, J. K., Brown, L. S., and Siebert, F. (1996) *Biochemistry 35*, 10807−10814.
24. Rothschild, K. J., He, Y.-W., Mogi, T., Marti, T., Stern, L. J., and Khorana, H. G. (1990) *Biochemistry 29*, 5954−5960.
25. Sakmar, T. P., Franke, R. R., and Khorana, H. G. (1989) *Proc. Natl. Acad. Sci. U.S.A. 86*, 8309−8313.
26. Sakmar, T. P., Franke, R. R., and Khorana, H. G. (1991) *Proc. Natl. Acad. Sci. U.S.A. 88*, 3079−3083.
27. Lin, S. W., and Sakmar, T. P. (1996) *Biochemistry 35*, 11149−11159.
28. Franke, R. R., Sakmar, T. P., Graham, R. M., and Khorana, H. G. (1992) *J. Biol. Chem. 267*, 14767−14774.
29. Kahlert, M., König, B., and Hofmann, K. P. (1990) *J. Biol. Chem. 265*, 18928−18932.
30. König, B., Arendt, A., McDowell, J. H., Kahlert, M., Hargrave, P. A., and Hofmann, K. P. (1989) *Proc. Natl. Acad. Sci. U.S.A. 86*, 6878−6882.
31. Ferretti, L., Karnik, S. S., Khorana, H. G., Nassal, M., and Oprian, D. D. (1986) *Proc. Natl. Acad. Sci. U.S.A. 83*, 599−603.
32. Ganter, U. M., Schmid, E. D., Perez-Sala, D., Rando, R. R., and Siebert, F. (1989) *Biochemistry 28*, 5954−5962.
33. Siebert, F., Mäntele, W., and Gerwert, K. (1983) *Eur. J. Biochem. 136*, 119−127.
34. Nakayama, T. A., and Khorana, H. G. (1991) *J. Biol. Chem. 266*, 4269−4275.
35. Weitz, C. J., and Nathans, J. (1992) *Neuron 8*, 465−472.

36. Min, K. C., Zvyaga, T. A., Cypess, A. M., and Sakmar, T. P. (1993) *J. Biol. Chem. 268*, 9400−9404.
37. Cohen, G. B., Oprian, D. D., and Robinson, P. R. (1992) *Biochemistry 31*, 12592−12601.
38. Herzyk, P., and Hubbard, R. E. (1995) *Biophys. J. 69*, 2419−2442.
39. Schertler, G. F. X., Villa, C., and Henderson, R. (1993) *Nature 362*, 770−772.
40. Baldwin, J. M., Schertler, G. F. X., and Unger, V. M. (1997) *J. Mol. Biol. 272*, 144−164.
41. Zhang, H., Lerro, K. A., Yamamoto, T., Lien, T. H., Sastry, L., Gawinowicz, M. A., and Nakanishi, K. (1994) *J. Am. Chem. Soc. 116*, 10165−10173.
42. Han, M., Lin, S. W., Smith, S. O., and Sakmar, T. P. (1996) *J. Biol. Chem. 271*, 32330−32336.
43. Han, M., Lin, S. W., Minkova, M., Smith, S. O., and Sakmar, T. P. (1996) *J. Biol. Chem. 271*, 32337−32342.
44. Jäger, S., Lewis, J. W., Zvyaga, T. A., Szundi, I., Sakmar, T. P., and Kliger, D. S. (1997) *Proc. Natl. Acad. Sci. U.S.A. 94*, 8557−8562.
45. Rath, P., DeCaluwé, L. L. J., Bovee-Geurts, P. H. M., DeGrip, W. J., and Rothschild, K. J. (1993) *Biochemistry 32*, 10277−10282.
46. Ganter, U. M., Gärtner, W., and Siebert. F. (1988) *Biochemistry 27*, 7480−7488.
47. Majoube, M., Millie, Ph., and Vergoten, G. (1995) *J. Mol. Struct. 344*, 21−36.

BI9801560